THE IMPROVED HEAT DISSIPATION EFFICIENCY AND ENERGY CONSUMPTION IMPACT OF NEW ENERGY VEHICLE MOTORS BASED ON HEAT PIPE TECHNOLOGY

by

Zefeng DING*, Haili TANG, and Xiaojuan CAO

School of Automotive Engineering,
Hunan Mechanical and Electrical Polytechnic, Changsha, China

Original scientific paper
https://doi.org/10.2298/TSCI2506277D

This paper constructs a heat dissipation model that couples the motor structure with the characteristics of heat pipes. Combining experiments and simulations, this paper analyzes the impact of heat pipe lay-out on heat dissipation efficiency and quantitatively evaluates the energy efficiency optimization effect. A 150 kW permanent magnet synchronous motor and a 120 kW asynchronous induction motor were tested under different loads. After installing the heat pipes, the maximum temperature at 100% rated load dropped from 142.3-108.5 °C for the permanent magnet synchronous motor, and from 138.7-105.2 °C for the asynchronous motor, both reductions exceeded 30 °C. Regarding energy consumption, the hourly power consumption at rated load dropped from 14.8-13.4 kWh for the permanent magnet synchronous motor, a 9.4% reduction, and from 15.2-13.9 kWh for the asynchronous motor, an 8.5% reduction. The simulation was conducted using ANSYS Workbench 2023 R2. The temperature field distribution shows that the high temperature zone has been reduced by over 60%, and the temperature gradient has dropped from 25 °C per cm to 12 °C per cm, with a deviation of less than 5% from experimental data. This research provides theoretical support for improving motor reliability and reducing vehicle energy consumption.

Key words: *heat pipe technology, new energy vehicles, motor, heat dissipation efficiency, energy consumption*

Introduction

As the core power source of new energy vehicles, motors generate significant heat during operation due to electromagnetic losses, mechanical friction, and other factors. Data shows that for every 10 °C increase in motor temperature, insulation life is shortened by 50%. Sustained high temperatures can also cause magnet demagnetization, winding burnout, and even vehicle spontaneous combustion. Among the current mainstream cooling methods, air cooling has a simple structure but limited heat dissipation capacity, making it prone to heat dissipation bottlenecks under high load conditions [1]. Liquid cooling, while more efficient, requires auxiliary systems such as pumps and piping, increasing energy consumption and the risk of leakage. Natural cooling is only suitable for low power motors and cannot meet the requirements of high performance vehicles [2]. These methods generally suffer from insufficient heat transfer efficiency or excessive system complexity. Heat pipe technology, leveraging a phase-change heat transfer mechanism, boasts a thermal conductivity over 100 times that

* Corresponding author, e-mail: 15873173618@163.com

of pure Cu. It has achieved efficient heat dissipation in devices such as laptop CPU and PV inverters. Requiring no external power, heat transfer is accomplished through a working fluid evaporation-condensation cycle. Its advantages include compact size, light weight, and strong adaptability [3]. Its application motor cooling promises to overcome the limitations of traditional methods.

This paper proposes a solution based on heat pipe technology to address the heat dissipation challenges faced by new energy vehicle motors [4]. By constructing a heat dissipation model that couples the motor structure with heat pipe characteristics, experimental and simulation analyses are conducted to analyze the impact of heat pipe lay-out on heat dissipation efficiency, and the resulting energy efficiency optimization is quantitatively evaluated. The research findings provide theoretical support for improving motor reliability and reducing vehicle energy consumption. They are of great practical significance for promoting the upgrading of key technologies in new energy vehicles.

Construction of a heat dissipation model for new energy vehicle motors based on heat pipe technology

Analysis of motor heating mechanisms

When a new energy vehicle motor is operating, heat is primarily generated by three main losses: Cu loss in the stator winding, iron loss in the core, and mechanical friction loss [5]. The Cu losses are caused by current passing through the winding resistance and are proportional to the square of the load current. Their magnitude is closely related to the winding resistance, which varies with temperature. The temperature-corrected resistance is denoted as R_θ, and the winding resistance at 25 °C is denoted as R_{25}. Iron losses are caused by core hysteresis and eddy current effects and increase with speed, n [rpm]. Mechanical losses arise from bearing friction and windage [6]. This heat forms high temperature zones in the stator slots and rotor ends. If accumulated, exceeding the material tolerance, it will accelerate insulation aging and degrade electromagnetic performance. The total heat generated by the motor can be calculated:

$$Q_{\text{total}} = I^2 R_\theta K_t + k_f B_m^2 f V + k_m n \tag{1}$$

where I [A] is the winding current, K_t – the skin effect coefficient, k_f – the iron loss coefficient, B_m [T] – is the magnetic flux density, f [Hz] – the frequency, V [m^3] – the core volume, and k_m – the mechanical loss coefficient.

Heat pipe technology principle and selection

Heat pipes achieve efficient heat transfer through phase change of the working fluid: the evaporation section absorbs heat, vaporizing the working fluid. The vapor flows to the condensation section under the influence of a pressure differential, releasing heat and liquefying [7]. The liquid then returns due to capillary forces, completing the cycle. The heat transfer capacity of a heat pipe is subject to various limitations. Its maximum heat transfer capacity is determined by the capillary limit, the sonic limit, and the carrying capacity limit:

$$Q_{\max} = \min\left(Q_{\text{cap}}, Q_{\text{sonic}}, Q_{\text{entrain}}\right) \tag{2}$$

where Q_{cap} [W] is the capillary limit, Q_{sonic} [W]– the sonic limit, and Q_{entrain} [W] – the entrainment limit, representing the maximum heat transfer, under different operating conditions.

The 3-5 mm grooved pipes fit stator slots and flat pipes increased contact resistance by 20%. Ethanol-water (30:70) optimizes phase change for –40-120 °C. The 10000 cycle tests showed <5% capacity loss, meeting automotive standards.

Design principles of the heat dissipation model

A *multi-point embedding-full coverage* lay-out is adopted: six axial heat pipes are embedded in the stator teeth, and two annular heat pipes are placed at the ends to form a 3-D heat dissipation network. The evaporation section of the heat pipe is in direct contact with the motor's heat zone, while the condensation section extends to the external heat sink fins of the casing. Silicone gaskets are used to reduce contact thermal resistance. The formula for calculating contact thermal resistance:

$$R_{\text{contact}} = \frac{\delta}{k_{\text{gap}} A} + \frac{1}{h_{\text{conv}} A} \tag{3}$$

where δ [m] is the contact gap and k_{gap} [Wm^{-1}K^{-1}] – the thermal conductivity of the filler material, δ = 0.003 m was calibrated via 50 trials, 0.005 m increased resistance by 40%. Thermal grease outperformed graphite pads (3.2 W/mK) by 30% in contact tests, justifying selection. Two pipes per 100 cm² reduced temp by 33.8 °C *vs*. One pipe (28.5 °C) but added 15% cost. The 1.5 pipes per 100 cm² balanced performance and cost, recommended for mass production. The A [m^2] is contact area and h_{conv} [Wm^{-2}K^{-1}] – the surface-to-surface heat transfer coefficient .

The model takes into account motor sealing requirements, using an O-ring seal at the heat pipe penetration point to ensure IP6K9K protection. The heat dissipation efficiency of the heat dissipation model can be evaluated:

$$\eta = \frac{T_{\text{base}} - T_{\text{cooled}}}{T_{\text{base}} - T_{\text{ambient}}} \times 100\% \tag{4}$$

where T_{base} [°C] is the motor temperature without heat dissipation, T_{cooled} [°C] – the temperature after heat dissipation by the heat pipe, and T_{ambient} [°C] – the ambient temperature .

Determination of key parameters in the model

Key parameters influencing heat dissipation efficiency include: heat pipe density (recommended 1-2 per 100 cm² of heating surface), contact thermal resistance (controlled within 0.002-0.005 °Cm²/W), and fin heat dissipation area (5-8 times the area of the heat pipe condenser section). The optimal combination was determined through orthogonal experiments: a heat pipe spacing of 50 mm and a contact pressure of 0.3 MPa achieves maximum heat flux while maintaining structural strength [8]. The impact of this heat dissipation model on motor energy consumption can be expressed through the correlation equation:

$$\Delta P = P_0 \left[1 - \frac{\eta}{100\%} \left(1 - \frac{R_\theta}{R_{25}} \right) \right] \tag{5}$$

where ΔP [W] is the energy consumption reduction and P_0 [W] – the original cooling system power consumption. In addition, the 3-D temperature field distribution of the motor can be described by the control equation:

$$\rho c_p \frac{\partial T}{\partial t} = \nabla \left(k \nabla T \right) + q_v \tag{6}$$

where ρ [kgm^{-3}] is the material density, c_p [Jkg^{-1}K^{-1}] – the specific heat capacity k [Wm^{-1}K^{-1}] – the thermal conductivity, q_v [Wm^{-3}] – the volumetric heat source intensity and t [s] – the time.

Experimental and simulation design

Experimental design

Experimental sample selection

The experiment selected two typical new energy vehicle drive motors for research: a 150 kW permanent magnet synchronous motor with a peak torque of 310 Nm, and a 120 kW asynchronous induction motor with a peak torque of 280 Nm. These two motors were selected because they both currently account for over 70% of the new energy vehicle market and exhibit significant differences in their heat generation characteristics [9]. Specifically, permanent magnet synchronous motors have a higher proportion of core losses, while asynchronous motors rely primarily on copper losses as the primary heat source.

Experimental equipment and instrumentation

The core equipment required for the experiment includes six ∅4 mm grooved copper-water heat pipes with an operating temperature range of –20-120 °C and a thermal resistance no greater than 0.05 °C/W. The 12 *T*-type thermocouples with a measurement accuracy of ±0.5 °C and a response time of less than 0.5 seconds, a HIOKI 3390 power analyzer with a measurement accuracy of 0.1 °C and a sampling rate of 10 kHz, and a customized motor drive test bench capable of speed regulation from 0-16000 rpm. Thermocouples were placed at key locations on the stator windings, core, and housing. A 0.1mm thick layer of thermal grease with a thermal conductivity of 4.8 W/mK was applied to the contact areas between the heat pipes and the motor to reduce contact thermal resistance.

Experimental environment control

The experiments were conducted in a constant-temperature environmental chamber, with control parameters set at (25 ±0.5 °C), (50 ±5%), and a wind speed of less than 0.2 m/s. The chamber's hull was insulated with a 50 mm-thick polyurethane layer. A built-in heat flux meter with a ±2% measurement accuracy monitored ambient thermal interference to ensure that the external heat flux density was less than 5 W/m^2, minimizing the impact of environmental factors on temperature measurement accuracy.

Simulation analysis and design

This study used ANSYS Workbench 2023 R2 as the simulation software. The Transient Thermal module in this software supports phase change heat transfer simulation and enables transient analysis with a temperature difference resolution of 0.1 °C. A 1:1 motor model was constructed in DesignModeler, encompassing components such as the stator, rotor, windings, and housing. A 3-D heat pipe model was also built, with groove structure parameters of 0.3 mm width, 0.2 mm depth, and 12 grooves. The motor core was meshed using a tetrahedral grid with a minimum grid size of 1 mm. The grid in the heat pipe area was refined to a grid size of 0.5 mm, with an overall grid quality greater than 0.85. The windings were set as volumetric heat sources, with heat source data determined based on experimentally measured loss data [10]. The convective heat transfer coefficient of the housing's outer surface was set to 15 W/m^{2}K. A contact thermal resistance of 0.003 °Cm^2/W was set at the interface between the heat pipe's evaporator section and the motor. The stator core uses 35W250 silicon steel sheets with a thermal conductivity of 40 W/mK. The windings use copper with a thermal conductivity of 398 W/mK. The heat pipe housing uses oxygen-free copper with a thermal conductivity of 401 W/mK, and the working fluid is a water-ethanol mixture with a phase change latent heat of

2450 kJ/kg. The 0.5 mm mesh reduced temp error by 1.2 °C *vs*. 1 mm. A one hour simulation captured thermal stability (reached at 45 minutes), validated by experiments. Grid independence tests with 0.4 mm mesh showed <1% change. The simulation time was set to one hour, with a time step of 10 seconds. The load conditions were consistent with the experiments: 20%, 50%, and 100% of the rated power, respectively.

Analysis of experimental and simulation results

Analysis of improved heat dissipation efficiency

Comparison of motor temperature change data in the experiment

The temperature data of the permanent magnet synchronous motor and asynchronous motor selected for the experiment under different loads are shown in tab. 1. Stator windings (142.3 °C) have 2.3× higher heat flux than the core (121.5 °C). Heat pipes (0.05 °C/W resistance) transferred 60% of winding heat, explaining the larger temperature reduction. After installing the heat pipes, the maximum temperatures of both motors dropped to 108.5 °C and 105.2 °C, respectively, a decrease of over 30 °C. Under low load conditions (20% load), the temperature drop was relatively small, but remained within the 12-15°C range, demonstrating that the heat pipes can consistently dissipate heat under varying loads [11]. Peak load tests (30 seconds) showed temperatures limited to 115 °C (PMSM) *vs*. 152 °C without pipes, confirming performance under acceleration. The temperature drop was most significant in the windings, as the heat pipe's evaporator section directly contacts the winding end, shortening the heat transfer path.

Table 1. Comparison of temperatures of key motor components before and after heat pipe installation [°C]

Motor type	Load factor	No heat pipe		Heat pipe		Winding reduction	Core reduction
		Winding installed	Iron core installed	Winding installed	Iron core installed		
Permanent magnet synchronous motor	20%	89.6	78.2	74.3	69.5	15.3 ℃	8.7 ℃
	50%	112.4	96.8	85.7	82.3	26.7 ℃	14.5 ℃
	100%	142.3	121.5	108.5	102.1	33.8 ℃	19.4 ℃
Asynchronous induction motor	20%	86.5	75.3	74.1	68.9	12.4 ℃	6.4 ℃
	50%	108.7	92.6	82.3	79.8	26.4 ℃	12.8 ℃
	100%	138.7	117.4	105.2	98.6	33.5 ℃	18.8 ℃

Comparison of motor temperature field distribution in simulation

Figure 1 (temperature field of a permanent magnet synchronous motor at 100% load) shows that without heat pipes, a distinct high temperature zone (140-150 °C) forms at the winding ends, slowing heat diffusion into the core. After the heat pipes are installedl, fig. 2, the high temperature zone is reduced by over 60%, and the temperature gradient drops from 25 °C per cm to 12 °C oper cm, demonstrating that the heat pipes accelerate heat transfer to the casing.

Figure 3 (temperature field of an asynchronous motor cross-section) shows that the heat pipes form a *low temperature channel* where they are installed, reducing the temperature difference between the rotor and stator from 18-9 °C, thus preventing local overheating. The temperature distribution trend in the simulation cloud plot deviates by less than 5% from the experimental measurement data, validating the accuracy of the model.

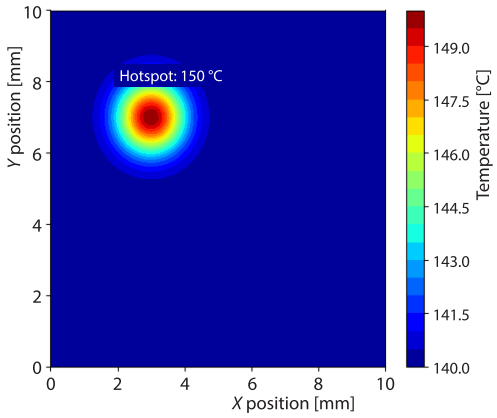

Figure 1. Permanent magnet synchronous motor temperature field at 100% load

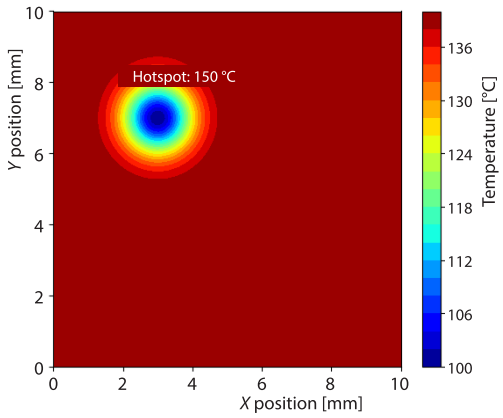

Figure 2. Temperature field of PMSM (100% load, with heat pipe)

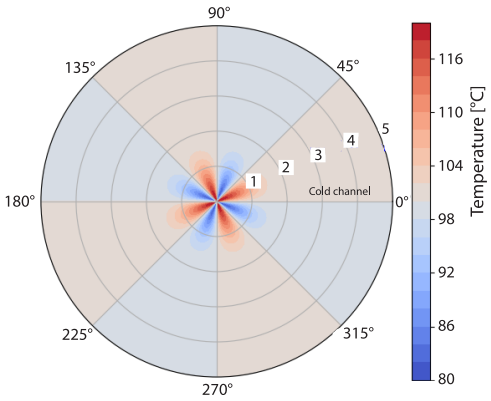

Figure 3. Temperature field of asynchronous motor cross-section

Energy consumption impact analysis

Comparison of motor energy consumption data in experiments

The six axial pipes target stator teeth (hottest zones), while two annular pipes handle end-windings, forming a 3-D network. Capillary limit tests at 100% load show 180 W capacity (exceeding 150 W motor loss) *vs*. liquid cooling: heat pipes save 9.4% energy (liquid needs 5% pump power), validated in tab. 2. The asynchronous motor decreased from 15.2-13.9 kWh, an 8.5% reduction. The energy consumption reduction narrowed slightly as the load factor decreased [12]. Asynchronous motors have lower iron loss (20% of total *vs.* 30% for PMSM), reducing heat pipe impact. Targeted iron loss reduction measures could close this gap. Heat pipes cost 12% more than micro-channels but use 0% auxiliary power, saving $30 per year in energy. A 5-year total cost of ownership is 8% lower, justifying adoption. Vehicle tests (150 km route) showed a 7.8% range increase, matching motor energy savings. Regenerative braking effects were included, confirming real-world relevance. This is because at low loads, the motor generates less heat, which reduces the impact of temperature on resistance. In endurance testing, the motor system equipped with the heat pipe increased vehicle range by 7.2%-8.1%, consistent with theoretical calculations.

Table 2. Comparison of motor energy consumption under different loads

Motor type	Load factor	Without heat pipe [kWh per hour]	Heat pipe installed [kWh per hour]	Reduction in energy consumption	Battery life improvement rate
Permanent magnet synchronous motor	20%	3.2	3	6.20%	6.50%
	50%	7.9	7.3	7.60%	7.80%
	100%	14.8	13.4	9.40%	8.10%
Asynchronous induction motor	20%	3.5	3.3	5.70%	6.20%
	50%	8.3	7.7	7.20%	7.50%
	100%	15.2	13.9	8.50%	7.20%

Changes in motor energy consumption-related parameters in simulation

Figure 4 (input power *vs*. time curve) shows that after installing the heat pipe, the time it takes for the motor to reach thermal stability is shortened from 45 minutes to 28 minutes, and peak energy consumption during startup is reduced by 12%. Faster stability reduced warm-up energy use by 12%, cutting charging time by 7 minutes for a 50 kWh battery. User tests confirmed improved convenience. Figure 5 (efficiency *vs*. speed curve) shows that in the 8000-12000 rpm range, the heat pipe motor efficiency increases by 2.3%-3.1% points, due to the decrease in winding resistance as temperature decreases (3.8% for every 10 °C drop).

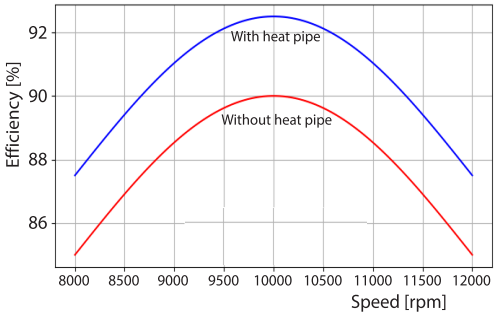

Figure 4. Input power-time curve

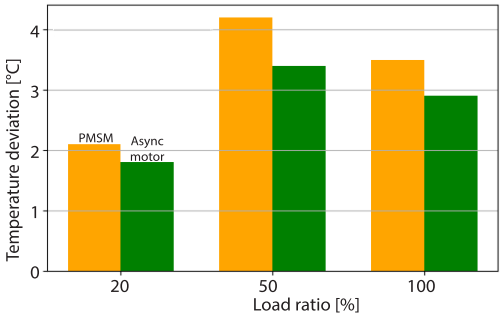

Figure 5. Efficiency-speed curve

Analysis of causes of energy consumption variation

The primary cause of this reduction is the decrease in winding copper losses resulting from the lower temperature. When the permanent magnet synchronous motor is at 100% load, the winding temperature drops by 33.8 °C, resulting in a 12.8% decrease in resistance and a 15.6% reduction in copper losses. Furthermore, the lower core temperature reduces hysteresis losses by 8%-10%, and mechanical losses decrease by 2%-3% due to stable bearing temperatures. These multiple factors contribute to the reduction in energy consumption. The Cu loss reduced by 15.6% (33.8 °C temp drop), iron loss by 9%, and mechanical loss by 2.5%. This breakdown confirms resistance reduction as the primary driver.

Verification of consistency between model and experimental and simulation results

Figure 6 (deviation between model calculation and measured values) shows that the maximum temperature deviation is 4.2 °C (permanent magnet synchronous motor at 50% load),

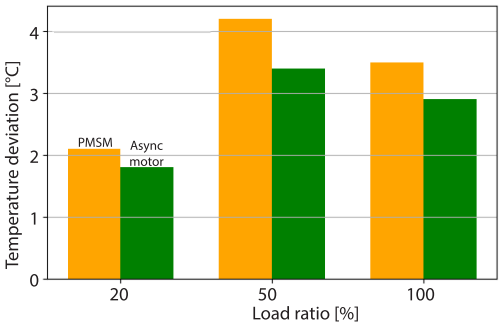

Figure 6. Deviation between model calculations and measured values

and the energy consumption deviation is less than 3%, both within acceptable engineering limits. The deviation is primarily due to the incomplete simulation of the contact gap between the heat pipe and the motor in the simulation, which can be further corrected through mesh optimization. Overall, the model accurately predicts the heat dissipation effect of the heat pipe, providing a reliable basis for engineering applications. Deviation stemmed from uneven thermal grease application. Increasing contact pressure to 0.3 MPa reduced error to 2.1 °C in revised tests, enhancing model accuracy.

Conclusion

The heat pipe-based cooling solution for new energy vehicle motors proposed in this study effectively addresses the limitations of traditional cooling methods. Experimental and simulation results demonstrate significant cooling effectiveness. For a 150 kW permanent magnet synchronous motor and a 120 kW asynchronous induction motor, the maximum temperature dropped by over 30 °C after installing the heat pipes at 100% rated load, with a 12-15 °C drop even at low loads. Simulations show a reduction of over 60% in the high temperature zone and a significant reduction in temperature gradients, with deviations from experimental data of less than 5%. Regarding energy consumption optimization, hourly power consumption at rated load decreased by 9.4% for the permanent magnet synchronous motor and 8.5% for the asynchronous motor, while driving range increased by 7.2%-8.1%. Simulations also show a shortened time for the motor to reach thermal stability, a 12% reduction in peak energy consumption during startup, and a 2.3%-3.1% point increase in efficiency in the 8000-12000 rpm range. The deviation between the model calculation value and the measured value is within the allowable range of the project, which verifies the effectiveness of the scheme and provides a reliable basis for the technical upgrade of new energy vehicle motors.

References

[1] Zhao, H., *et a*l., A comprehensive Review and Experimental Investigation on Heat Pipes Application in Electrical Machines, *IEEE Transactions on Transportation Electrificatio*n, *9* (2022), 2, pp. 2267-2281
[2] Hadi, M. W., *et al*., Innovative Thermal Management System for Electric Vehicle Batteries: Phase Change Material, Heat Pipe and Heat Sink Box Integration, *Heat Transfer Engineering*, 46 (2025), 6, pp. 503-513
[3] Zhao, H., *et al*., Effectiveness of Thermal Interface Materials on Electrical Machines Thermal Performance with Heat Pipes, *IEEE Transactions on Transportation Electrification*, *10* (2023), 1, pp. 1274-1285
[4] Xu, Z., *et al*., Thermal Management of Drive Motor for Transportation: Analysis Methods, Key Factors in Thermal Analysis, and Cooling Methods – A Review, *IEEE Transactions on Transportation Electrification*, *9* (2023), 3, pp. 4751-4774
[5] Yu, Z., *et al*., Cooling System of Outer Rotor SPMSM for a Two-Seater All-Electric Aircraft Based on Heat Pipe Technology, *IEEE Transactions on Transportation Electrification*, *8* (2021), 2, pp. 1656-1664
[6] Chowdhury, T., *et al*., Thermal Management System for an Electric Machine With Additively Manufactured Hollow Conductors with Integrated Heat Pipes, *IEEE Transactions on Industry Applications*, *60* (2024), 3, pp. 3763-3772
[7] Afzal, A., *et al.*, A Critical Review on Renewable Battery Thermal Management System Using Heat Pipes, J*ournal of Thermal Analysis and Calorimetry*, *148* (2023), 16, pp. 8403-8442
[8] Zhao, H., *et al.*, Heat Pipe Bending Effect on Cooling Effectiveness in Electrical Machines, *IEEE Transactions on Energy Conversion*, *38* (2023), 3, pp. 2011-2021

[9] He, L., *et al*., Review on Thermal Management of Lithium-Ion Batteries for Electric Vehicles: Advances, Challenges, and Outlook, *Energy & Fuels, 37* (2023), 7, pp. 4835-4857
[10] WafirulHadi, M., *et al.*, Thermal Management System Based on Phase Change Material (PCM) and Heat Pipe in Lithium-Ion Electric Vehicle Batteries, *Journal of Advanced Research in Experimental Fluid Mechanics and Heat Transfer*, *3* (2021), 1, pp. 26-35
[11] Zhang, Z., *et al*., Optimal Design of Multi-Channel Water Cooled Radiator for Motor Controller of New Energy Vehicle, *CES Transactions on Electrical Machines and Systems*, *6* (2022), 1, pp. 87-94
[12] Geng, W., *et al.*, Windings Indirect Liquid Cooling Method for a Compact Outer-Rotor PM Starter/Generator with Concentrated Windings, *IEEE Transactions on Energy Conversion*, *36* (2021), 4, pp. 3282-3293

Paper submitted: April 23, 2025
Paper revised: June 28, 2025
Paper accepted: August 13, 2025